

**The Brittle-Ductile Transition Stress of Different Rock Types and Its
Relationship with Uniaxial Compressive Strength and Hoek-Brown Material
Constant (m_i)**

**Seyed Morteza Davarpanah¹, Mohammad Sharghi², Abolfazl Tarifard³, Ákos Török⁴, and
Balázs Vásárhelyi⁵**

¹ Budapest Univ. of Technology and Economics, Dept. of Engng Geol. & Geotechnics. e-mail: morteza.davarpanah@emk.bme.hu, <https://orcid.org/0000-0002-8046-5814>

² Sahand Univ. of Technology, Dept. of Mining Eng. e-mail: m_sharghi@sut.ac.ir, <https://orcid.org/0000-0003-3451-8513>

³ Budapest Univ. of Technology and Economics, Dept. of Engng Geol. & Geotechnics. e-mail: abolfazl.tarifard.karvigh@emk.bme.hu, <https://orcid.org/0000-0003-0912-9321>

⁴ Budapest Univ. of Technology and Economics, Dept. of Engng. Geol. & Geotechnics. e-mail: torok.akos@emk.bme.hu, <https://orcid.org/0000-0002-0568-1031>

⁵ Budapest Univ. of Technology and Economics, Dept. of Engng. Geol. & Geotechnics. e-mail: vasarhelyi.balazs@emk.bme.hu, <https://orcid.org/0000-0002-5394-4510>

Corresponding author: Seyed Morteza Davarpanah (morteza.davarpanah@emk.bme.hu)

Key Points:

Brittle-ductile transition stress, Hoek-Brown material constant (m_i), uniaxial compressive strength.

Abstract

The investigation on brittle-ductile transition has become of central importance in many geologic situations. This paper aims to study the relationship between brittle-ductile transition stress, uniaxial compressive strength and Hoek-Brown material constant (m_i). To fulfill this goal, significant amount of data from literature were selected and analyzed. Additionally, transition stress was determined based on the combination of Hoek-Brown failure criteria and the recently used transition-ductile stress limit. New non-linear correlations were established between uniaxial compressive strength and Hoek-Brown material constant (m_i) for different rock types. The obtained results demonstrate good correlation between uniaxial compressive strength and transition stress for igneous, sedimentary and metamorphic rocks; however, the correlation was not notable between Hoek-Brown material constant (m_i) and transition stress for sedimentary and metamorphic rocks.

1 Introduction

The study of the brittle-ductile transition behaviour of rocks that are found at deeper subsurface regions has the significance of academic research and also in the engineering application such as tunnelling, deep foundation or even in hydrocarbon exploration. The mechanical behaviour of rocks in the brittle-ductile transition region is obviously restricted by strain rate, temperature, effective stress, the microstructure and mineralogy of the rock and water (Heard, 1960, Mogi 1966, Byerlee 1968, Mogi 1972, Evans and Fredrich 1990, Jaeger et al. 2007, Schopfer et al., 2013, Lyakhovsky et al., 2015, Liu et al., 2018, Aharonov and Scholz, 2019, You et al. 2021).

Kármán (1910, 1911) was the first, who investigated the influence of the confining pressure for the mechanical behaviour of the rock. According to literatures, the brittle material becomes ductile due to increasing the confining pressure (Evans and Fredrich, 1990; Ledniczky and Vásárhelyi, 2000; Vásárhelyi, 2010; Ván and Vásárhelyi, 2010; Deák et al., 2012; Erarslan and Ghamgosar 2014; Mikelić et al. 2019). However, some rocks still exhibit brittleness even under high confining pressure at 1000 MPa or above (Paterson, 1982).

Mogi (1966, 2007) showed that the brittle-ductile transition pressures of silicate rocks are appreciably higher than those of carbonate rocks. This difference between silicate rocks and carbonate rocks suggests that there are different mechanisms of the brittle-ductile transition in different rock types. The transition boundary in carbonate rocks is somewhat different from that in silicate rocks, which is attributed to a different transition mechanism. However, Byerlee (1968) discussed this problem based on his measurement of friction of rocks, and he argued that the brittle-ductile transition boundary is independent of rock type.

Some carbonate rocks, particularly at high temperature follow the A-type brittle-ductile transitions while silicate rocks are considered to have B-type stress-strain curves (The typical stress-strain curves of A-type and B-type are schematically shown in Figures 1 and 2, respectively). Thus, the pressure dependence of the strength of rocks near the transition pressure is different between A-type and B-type. Most rocks, however, behave in an intermediate manner between A-type and B-type. An inelastic deformation takes place just before the transition pressure reached and after yielding both fracturing and plastic deformation likely occur. In addition, it was also suggested that a frictional sliding hypothesis is applicable for the brittle-

64 ductile transition process of rocks (noted as B-type) in which the permanent deformation in the
 65 post-yield region occurs by cataclastic flow or frictional sliding (Mogi, 1972).

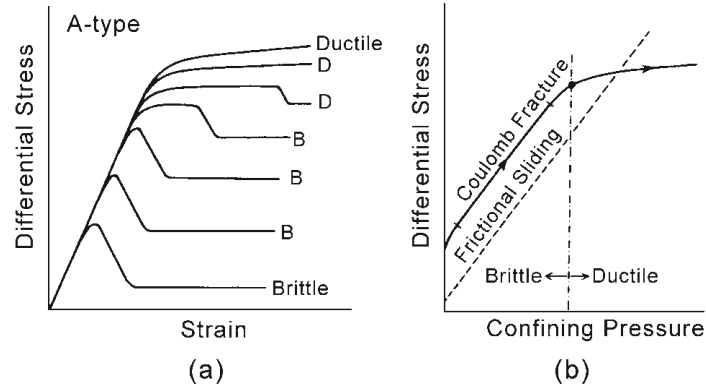


Figure 1. (a) Typical stress-strain curves of A-type rocks for different confining pressures. (b) Strength versus pressure curve and the failure behaviour in A-type rocks (Mogi, 2007).

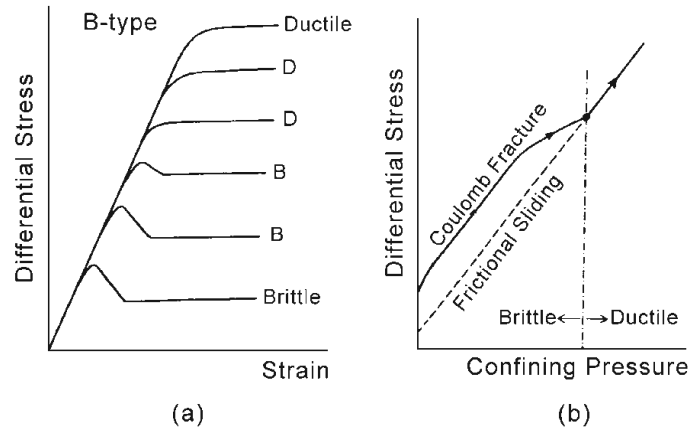


Figure 2. (a) Typical stress-strain curves of B-type rocks for different confining pressures. (b) Strength versus pressure curve and the failure behaviour in B-type rocks (Mogi, 2007).

66 With the increase of confining pressure, ductility, which is defined as the ability to
 67 undergo large permanent deformation without fracture (Mogi, 2007), increases markedly and a
 68 transition from the brittle to the ductile state takes place at some confining pressure. Figure 3
 69 shows the brittle-ductile behaviour in the conventional triaxial compression test as functions of
 70 the confining pressure and compressive strength of silicate rocks and carbonate rocks are given
 71 by Mogi (1966).

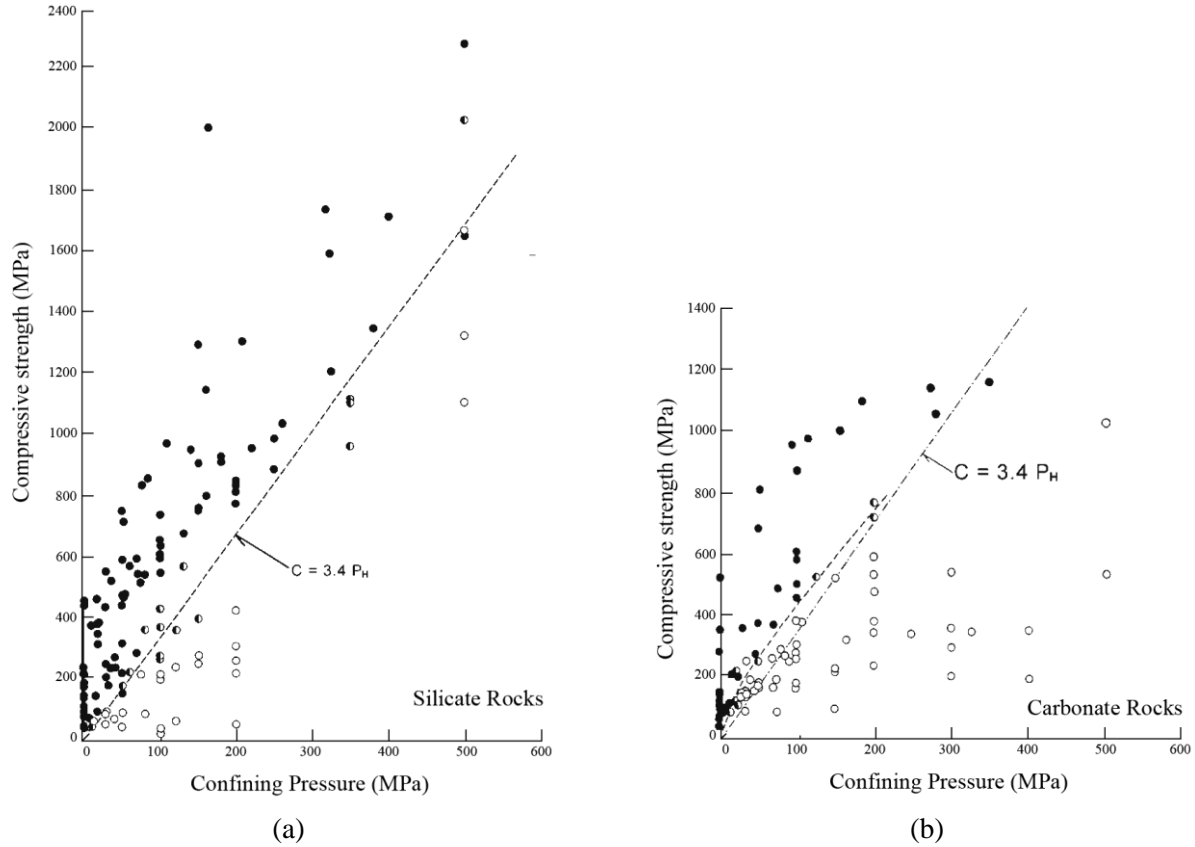


Figure 3. Failure behaviour of rocks at various strength and pressure. (a) silicate rocks. (b) carbonate rocks. Dotted line: the boundary between the brittle region and ductile region; closed circle: brittle; semi-closed circle: transition; open circle: ductile (after Mogi, 2007).

The goal of this research is to determine the transition stress limit based on Hoek-brown failure criteria and Mogi 1966 equation. In other words, by substituting Mogi, 1966 equation in Hoek-brown criteria, we have obtained square equation formula where transition stress can be derived. For this purpose, first, large data base for different rock types were collected from literature and transition stress was calculated for different rock types based on proposed square equation. Then, new non-linear correlations between Hoek material constant(m_i), uniaxial compressive strength (σ_c) and transition stress (σ_{tr}) for each rock type were established.

2. Theoretical background

In this section, in order to calculate the transition stress (σ_{tr}), Mogi ductile-brittle transition stress equation and Hoek-Brown failure criteria are reformulated. The Hoek-Brown (HB) failure criterion is widely used in rock mechanics and rock engineering practice. This semi-empirical failure criterion was introduced by Hoek and Brown (1980) and the following form was suggested for intact rock (see also Eberhardt, 2012):

$$\sigma_1 = \sigma_3 + \sigma_c \left(m_i \frac{\sigma_3}{\sigma_c} + 1 \right)^{0.5} \quad (1)$$

where σ_1 and σ_3 are major and minor principal stress at failure, respectively, m_i : Hoek- Brown material constant and σ_c : the uniaxial compressive strength of intact rock.

According to Eq. (1), two independent parameters are necessary, namely the:

- Uniaxial compressive strength of the intact rock (σ_c),
- Hoek–Brown material constant of the intact rock (m_i).

It should be noted that the Hoek-Brown criterion is proposed to deal with shear failure in rocks. Therefore, the Hoek-Brown criterion is only applicable for confining stresses within the range defined by $\sigma_3 = 0$ and the transition from shear to a ductile failure, as shown in Figure 4. It was indicated that the range of confining stress σ_3 can have a significant influence on the calculation of m_i (Singh et al. 2011; Peng et al. 2013). Additionally, triaxial test data of Indiana limestone shows (Schwartz, 1964) that the applicability of the Hoek-Brown criterion is determined by the transition from shear to ductile failure at approximately $\sigma_1 = 4.0 \sigma_3$ (Hoek and Brown, 2019) (Figure 4). Mogi (1966) found that the average transition is defined as $\sigma_1 = 4.4 \sigma_3$, which is a convenient guide for the selection of the maximum confining pressure for triaxial tests of intact rocks. Typical stress-strain curves in the brittle, the transition and the ductile state are very different (see Figure 5).

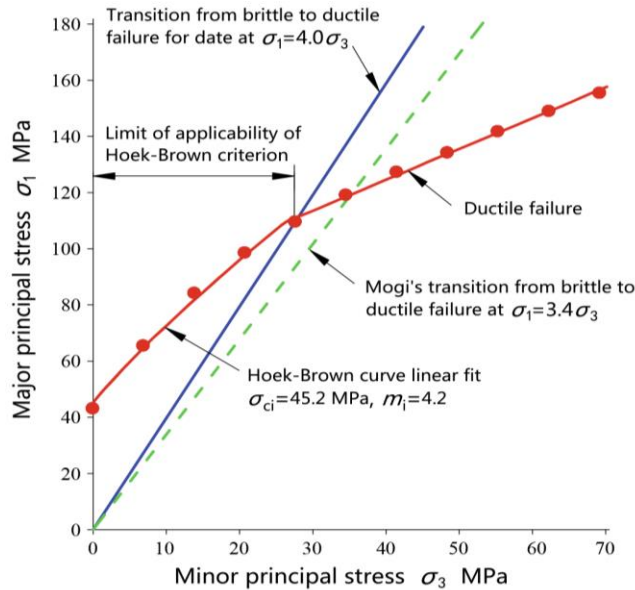


Figure 4. Limit of applicability of the HB criterion (Hoek and Brown, 2019).

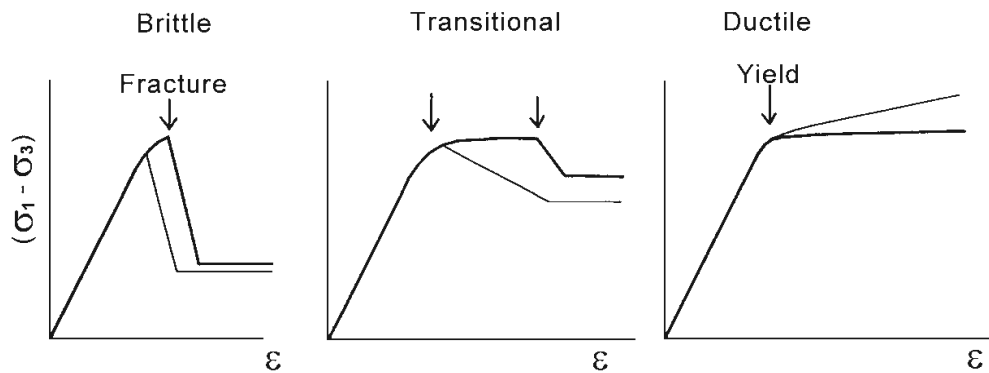


Figure 5. Typical stress-strain curves in brittle, transition, and ductile states (Mogi, 2007).

An empirical failure criterion has also been proposed, namely, for most rocks, the confining pressure must always be smaller than the uniaxial compressive strength to keep brittle behaviour of rock (Mogi, 1966). Figure 5 illustrates the comparison of two criteria (Eq. 2 and Eq. 3) according to Zuo and Shen (2020). However, most experimental data in Figure 6 shows that the brittle-ductile transition relationship may be nonlinear. The critical transition condition of brittle-ductile transition for rocks can be expressed by Eq. 2.

$$\bar{\sigma}_3^* = \frac{1}{\mu} \left[\frac{\bar{\sigma}_c^2}{4\beta} \left(\sqrt{1 + \mu^2} - \mu \right)^2 - \beta \right] \quad (2)$$

$$\bar{\sigma}_3^* \leq \bar{\sigma}_c \quad (3)$$

In Eq. 2, $\bar{\sigma}_c = \frac{\sigma_c}{\sigma_t}$, μ is the friction coefficient, β is the fracture parameter of rocks. Eq. 2 indicated that by increasing $\bar{\sigma}_c$, the required σ_3 to initiate the brittle-ductile transition stress increases. Figure 6 illustrates the comparison of two criteria (Eq. 2 and Eq. 3) (Zuo and Shen, 2020).

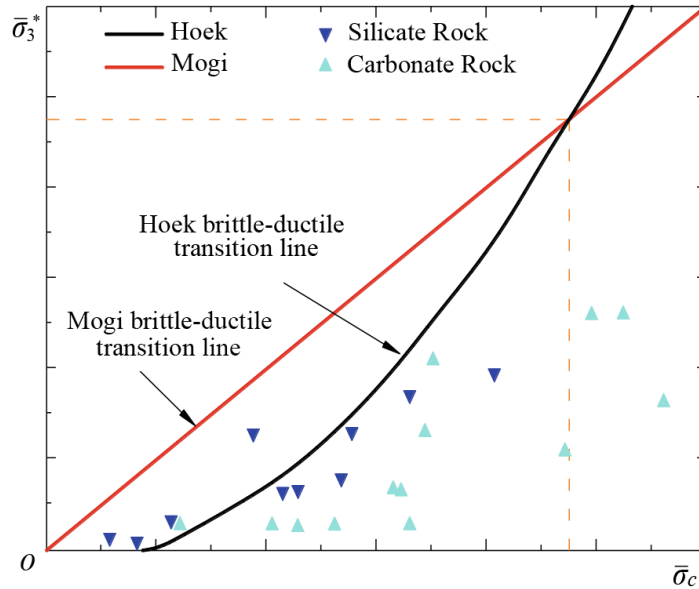


Figure 6. The relationship between the confining pressure at brittleness ductility transition and the value of UCS (Zuo and Shen, 2020).

In this paper, based on the above listed analyses, the transition point from brittle to ductile failure is calculated using σ_{TR} (transition stress) as referred to Mogi's widely used brittle-ductile transition limit (Mogi, 1966):

$$\sigma_1 - \sigma_3 = 3.4 \sigma_3 \quad (4a)$$

thus:

$$\sigma_1 = 4.4 \sigma_3 \quad (4b)$$

substituting Eq. 4 with Eq. 1 we have the following equations:

$$4.4 \sigma_3 = \sigma_3 + \sigma_c \left(m_i \frac{\sigma_3}{\sigma_c} + 1 \right)^{0.5} \quad (5)$$

116 σ_3 can be derived from the following equation.

$$11.56 \sigma_3^2 - m_i \sigma_3 \sigma_c - \sigma_c^2 = 0 \quad (6)$$

117 without taking into account the negative value, the transition stress (σ_{TR}) point can be calculated
118 from Eq. (4), using the equation 6:

$$\sigma_{TR} = \sigma_c \frac{m_i + \sqrt{m_i^2 + 46.24}}{23.12} \quad (7)$$

119 where, σ_c and σ_{TR} is the uniaxial compressive strength and transient stress, respectively, m_i is the
120 Hoek-Brown material constant.

121 3 Transition stress for different rock types

122 Through collecting the published data by Sheorey (1997) σ_{TR} was calculated for different
123 rock types. The data used in this paper is illustrated in Tables 1, 2 and 3 for igneous, sedimentary
124 and metamorphic rocks, respectively (see Appendix). The correlations between σ_{TR} and the
125 uniaxial compressive strength (UCS) are shown in Figure 7. As shown in Figure 7, for sandstone,
126 shale and gneiss, high determination correlation was observed. ($R^2 > 0.7$); however, the
127 correlation was weak for slate ($R^2 < 0.5$).

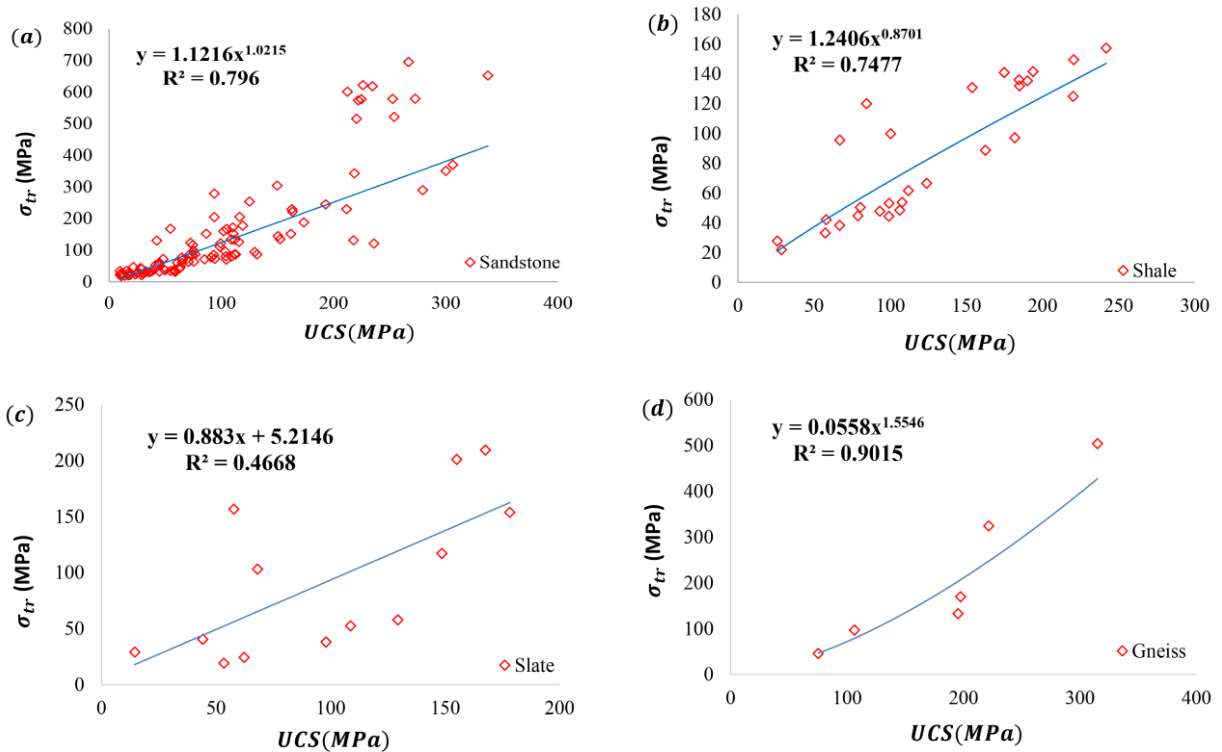


Figure 7. Relationship between σ_{TR} and UCS for. (a) sandstone. (b) shale. (c) slate. (d) gneiss.

Figure 8 displays the relationship between σ_{TR} and m_i values. As shown, we can see better correlation for gneiss with high determination coefficient ($R^2=0.88$).

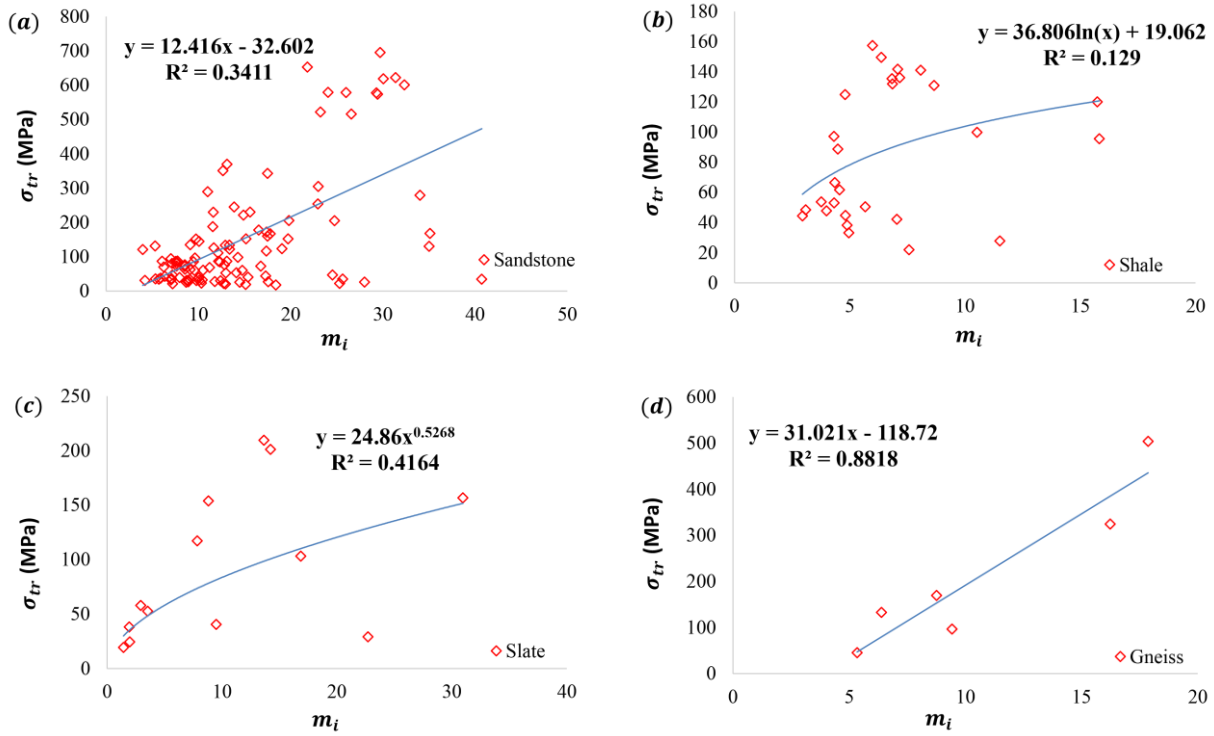


Figure 8. Relationship between σ_{TR} and m_i for. (a) sandstone. (b) shale. (c) slate. (d) gneiss.

Figure 9 exhibits the comparison of relationship between σ_{TR} and uniaxial compressive strength (UCS) for all the investigated rocks. Likewise, Figure 10 shows the comparison of relationship between σ_{TR} and published m_i values.

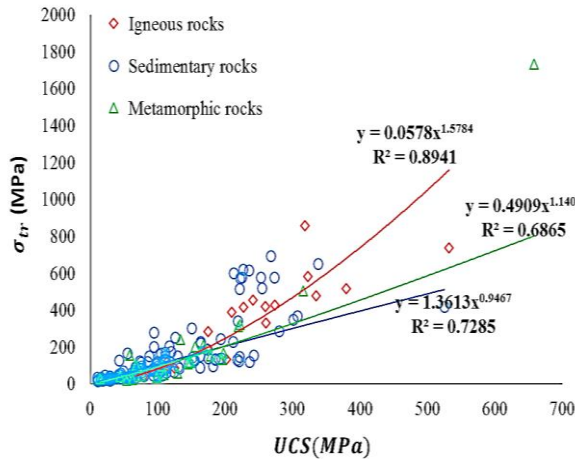


Figure 9. Relationship between σ_{TR} and UCS

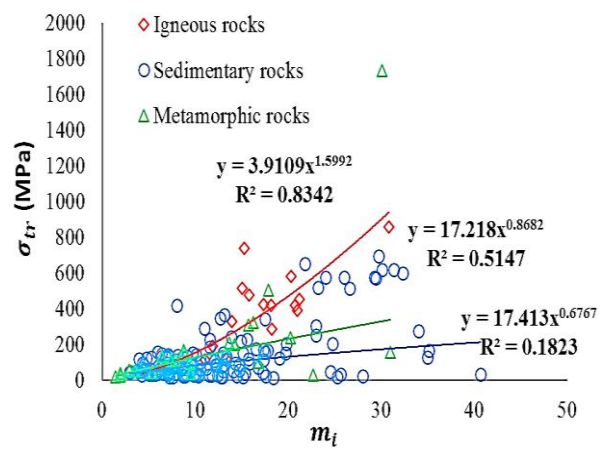


Figure 10. Relationship between σ_{TR} and m_i

4. Discussion and conclusion

According to this research results (Eq. 7), the value of σ_{tr} is influenced non-linearly by the value of m_i . In other words, as m_i increases, σ_{tr} increases. In fact, our proposed formula (Eq. 7) is in good agreement with the empirical failure criterion proposed by Mogi (1966) (Eq. 2) which suggests that by increasing the rigidity of rock, the required confining pressure σ_3 that triggers brittle-ductile transition increases. Similarly, Hu et al. (2018), proposed a micromechanics-based frictional damage model to investigate the brittle-ductile transition process of various rocks and found that critical damage at failure can be linearly related to the level of confining pressure. Figure 9 shows that σ_{tr} calculated by this research has a high correlation with UCS in most types of rocks and it can be used to estimate the transition stress of rocks based on their UCS. Figures 9 and 10 indicate that the best correlation was observed for igneous rocks and the reason is probably related to the texture and the origin of the igneous rocks.

In this research, new equation was proposed based on Mogi transition stress limit and Hoek-Brown criteria. The suggested equation is used to calculate σ_{tr} for various types of igneous, sedimentary and metamorphic rocks. The analyses of the relationships between uniaxial compressive strength (UCS), Hoek-Brown material constant (m_i) and brittle-ductile transition stress σ_{tr} showed that there is a new non-linear correlation between uniaxial compressive strength and transition stress. The result of this research reveals that the relation between the transition stress and UCS and m_i is rock type dependent. It means that for different rock types, the proposed formula has different material coefficients. Regression analysis shows that the determination coefficient between σ_{tr} and UCS for gneiss is 0.9, for sandstone is 0.8, for shale is 0.74. Similarly, the determination coefficient between σ_{tr} and m_i for gneiss is 0.88. The result of this research can be used to estimate σ_{tr} for different rock types in engineering practice.

Acknowledgments

We would like to state that data used in section. 3 is available through Sheorey (1997).

References

- Aharonov, E., & Scholz, C. H. (2019). The brittle-ductile transition predicted by a physics-based friction law. *Journal of Geophysical Research: Solid Earth*, 124(3), 2721-2737. <https://doi.org/10.1029/2018JB016878>
- Byerlee, J. D. (1968). Brittle-ductile transition in rocks. *Journal of Geophysical Research*, 73(14), 4741-4750. <https://doi.org/10.1029/JB073i014p04741>
- Deák, F., Ván, P., & Vásárhelyi, B. (2012). Hundred years after the first triaxial test. *Periodica Polytechnica Civil Engineering*, 56(1), 115-122. <https://doi.org/10.3311/pp.ci.2012-1.13>
- Eberhardt, E. (2012). The Hoek-Brown failure criterion. *Rock Mechanics and Rock Engineering*, 45, 981-988. <https://doi.org/10.1007/s00603-012-0276-4>
- Erarslan, N., & Ghamgosar, M. (2014). *Fracturing and indirect tensile strength of brittle and ductile rocks*. 2014 ISRM European Regional Symposium on Rock Engineering and Rock Mechanics: Structures in and on Rock Masses, EUROCK 2014, Vigo, Spain, 26-28 May 2014. London, United Kingdom: Taylor and Francis.

- Evans, B., & Fredrich, J. (1990). The brittle-ductile transition in rocks: recent experimental and theoretical progress. *Geophysical Monograph Series*, 56, 1-19. <https://doi.org/10.1029/GM056>
- Handin, J. (1953). An application of high pressure in geophysics: experimental rock deformation. *Transactions of the American Society of Mechanical Engineers*, 75, 315–324.
- Heard, H. C. (1960). *Transition from brittle fracture to ductile flow in Solnhofen limestone as a function of temperature, confining pressure, and interstitial fluid pressure*. In: Griggs, D., & Handin, J. (eds.) *Rock deformation*. Geological Society of America Memoirs, 79, 193–226.
- Hoek, E., & Brown, E. T. (1980). *Underground excavation in rock*. Institution of Mining & Metallurgy, London, England.
- Hoek, E., & Brown, E. T. (2019). The Hoek-Brown failure criterion and GSI – 2018 edition. *Journal of Rock Mechanics and Geotechnical Engineering*, 11, 445-463. <https://doi.org/10.1016/j.jrmge.2018.08.001>
- Hu, K., Zhu, Q., Chen, L., Shao, J., & Liu, J. (2018). A micromechanics-based elastoplastic damage model for rocks with a brittle–ductile transition in mechanical response. *Rock Mechanics and Rock Engineering*, 51, 1729-1737. <https://doi.org/10.1007/s00603-018-1427-z>
- Jaeger, J. C., Cook, N. G. W., & Zimmerman, R. W. (2007). *Fundamentals of rock mechanics*. 4th edn., Wiley-Blackwell, Oxford.
- Kármán, T. (1910). Mitől függ az anyag igénybevétele? (What influences the strength of the materials?). *Magyar Mérnök- és építész-Egyelet Közlönye*, 10, 212–226. (in Hungarian).
- Kármán, von T. (1911). Festigkeits Versuche unter allseitigem Druck. *Z. Verhandl. Deut. Ingr.* 55, 1749–1759. (in German).
- Ledniczky, K., & Vásárhelyi, B. (2000). Brittle-ductile transition of anisotropic rocks during three-point bending test. *Acta Geodaetica et Geophysica Hungarica*, 35, 75-80. <https://doi.org/10.1007/BF03325596>
- Liu, W., Zhu, X., & Jing, J. (2018). The analysis of ductile-brittle failure mode transition in rock cutting, *Journal of Petroleum Science and Engineering*, 163, 311-319. <https://doi.org/10.1016/j.petrol.2017.12.067>
- Lyakhovsky, V., Zhu, W., & Shalev, E. (2015). Visco-poroelastic damage model for brittle-ductile failure of porous rocks. *Journal of Geophysical Research: Solid Earth*, 120(4), 2179–2199. <https://doi.org/10.1002/2014JB011805>
- Meng, F., Zhou, H., Zhang, C., Xu, R., & Lu, J. (2014). Evaluation methodology of brittleness of rock based on post-peak stress–strain curves. *Rock Mechanics and Rock Engineering*, 48, 1787-1805. <https://doi.org/10.1007/s00603-014-0694-6>
- Mikelić, A., Wheeler, M.F. & Wick, T. (2019). Phase-field modeling through iterative splitting of hydraulic fractures in a poroelastic medium. *GEM - International Journal on Geomathematics*, 10(2). <https://doi.org/10.1007/s13137-019-0113-y>
- Mogi, K. (1966). Pressure dependence of rock strength and transition from brittle fracture to ductile flow. *Bulletin of the Earthquake Research Institute*, 44, 215–232.
- Mogi, K. (1972). Fracture and flow of rocks. *Developments in Geotectonics*, 4, 541–568. <https://doi.org/10.1016/B978-0-444-41015-3.50034-3>

- Mogi, K. (2007). *Experimental rock mechanics: 3*. Geomechanics Research Series, Taylor & Francis Group.
- Paterson, M. S. (1982). *Experimental rock deformation-the brittle field (Chinese transition)*. Geological Publishing House.
- Peng, J., Rong, G., Cai, M., Wang, X., & Zhou, C. (2014). An empirical failure criterion for intact rocks. *Rock Mechanics and Rock Engineering*, 47, 347–356. <https://doi.org/10.1007/s00603-012-0355-6>
- Schopfer, M. P. J., Childs, C., & Manzocchi, T. (2013). Three-dimensional failure envelopes and the brittle-ductile transition. *Journal of Geophysical Research: Solid Earth*, 118(4), 1378–1392. <https://doi.org/10.1002/jgrb.50081>
- Schwartz, A. E. (1964). *Failure of rock in the triaxial shear test*. In: Proc. 6th Rock Mech. Symp. Rolla, USA: University of Missouri, 109-151.
- Sheorey, P. R. (1997). *Empirical rock failure criteria (1st ed.)*. Central Mining Research Institute, India.
- Singh, M., Raj, A., & Singh, B. (2011). Modified Mohr-Coulomb criterion for non-linear triaxial and polyaxial strength of intact rocks. *International Journal of Rock Mechanics and Mining Sciences*, 48(4), 546–555. <https://doi.org/10.1016/j.ijrmms.2011.02.004>
- You, T., Waisman, H., & Zhu, Q. Z. (2021). Brittle-ductile failure transition in geomaterials modeled by a modified phase-field method with a varying damage-driving energy coefficient. *International Journal of Plasticity*, 136. <https://doi.org/10.1016/j.ijplas.2020.102836>
- Ván, P., & Vásárhelyi, B. (2010). *Centenary of the first triaxial test - recalculation of the results of Kármán*, Eurock'2010 (Laussane), Rock Mechanics in Civil and Environmental Engineering (Zhao J, Labiouse V, Dudt J-P, Mathier J-F, eds.), Taylor & Francis, 59–62.
- Vásárhelyi, B. (2010). Tribute to the first triaxial test performed in 1910. *Acta Geodaetica et Geophysica Hungarica*, 45, 227–230. <https://doi.org/10.1556/AGeod.45.2010.2.7>
- Wang, Y., Li, C., Hu, Y., & Zhou, X. (2017). A new method to evaluate the brittleness for brittle rock using crack initiation stress level from uniaxial stress–strain curves. *Environmental Earth Sciences*, 76(799). <https://doi.org/10.1007/s12665-017-7117-4>
- Liu, W., Zh., X., & Jing, J. (2018). The analysis of ductile-brittle failure mode transition in rock cutting. *Journal of Petroleum Science and Engineering*, 163, 311-319. <https://doi.org/10.1016/j.petrol.2017.12.067>
- You, T., Waisman, H., & Zhu, Q. Z. (2021). Brittle-ductile failure transition in geomaterials modeled by a modified phase-field method with a varying damage-driving energy coefficient. *International Journal of Plasticity*, 136. <https://doi.org/10.1016/j.ijplas.2020.102836>
- Zuo, J., & Shen, J. (2020), *The Hoek-Brown Failure criterion—From theory to application*. Springer, Singapore. <https://doi.org/10.1007/978-981-15-1769-3>

Appendix

Table 1

Published Values of Triaxial Parameters for Hoek-Brown Criterion Using Data Set for Igneous Rocks with the Calculated Transition Stress (Sheorey, 1997)

NO	Rock name	σ_c (MPa)	σ_t (MPa)	m_i	σ_{TR}
1	agglomerate tuff	92	11.43	7.926	73.1
2	andesite	201.9	31.64	6.225	134.87
3	basalt	79.1	17.45	4.313	42.31
4	diabase	322.9	15.85	20.324	583.17
5	diabase	532.0	34.6	15.310	737.76
6	diorite	67.8	10.82	6.103	44.69
7	diorite	124.3	18.57	6.548	85.96
8	gabbro	379.1	25.1	15.033	517.04
9	gabbro	226.9	10.92	20.738	417.71
10	granite	241.3	11.34	21.227	454.18
11	granite	318.2	10.31	30.816	858.44
12	granite	260.0	18.56	13.936	331.1
13	granite breccia	334.9	21.06	15.837	479.06
14	granodiorite	113.1	10.16	11.043	117.46
15	granodiorite	259.1	14.23	18.15	420.61
16	lamprophyre	116.3	14.02	8.174	94.6
17	quartzdiorite	174.7	9.53	18.274	285.42
18	quartzdiorite	173.4	14.47	11.903	192.09
19	quartzdiorite	98.6	7.35	13.343	120.77
20	quartzdiorite	273.8	15.71	17.371	426.63
21	quartzdiorite	209.7	9.98	20.965	390.06
22	rhyolite	106.4	18.96	5.430	65.04

Table 2

Published Values of Triaxial Parameters for Hoek-Brown Criterion Using Data Set for Sedimentary Rocks with the Calculated Transition Stress (Sheorey, 1997)

NO	Rock name	σ_c (MPa)	σ_t (MPa)	m_i	σ_{TR}
1	dolomite	145.3	18.2	7.859	114.7
2	dolomite	524.5	64.22	8.044	421.44
3	limestone	65.9	4.47	14.663	87.86
4	limestone	128.8	9.85	12.992	154.07
5	limestone	94.9	13.15	7.076	69.33
6	limestone	53.6	7.84	6.686	37.61
7	sandstone	85.2	9.87	8.52	71.57
8	sandstone	75.5	8.72	8.543	63.55
9	sandstone	149.9	6.51	22.996	304.57
10	sandstone	129.9	18.15	7.017	94.33
11	sandstone	112.9	14.68	7.561	86.58
12	sandstone	109	8.11	13.367	133.72
13	sandstone	21.7	0.88	24.537	46.93
14	sandstone	152.4	16.54	9.11	134.98
15	sandstone	74.2	5.98	12.33	84.76
16	sandstone	300.2	23.57	12.658	350.93
17	sandstone	74.6	4.28	17.378	116.29
18	sandstone	94.3	12.13	7.652	72.96
19	sandstone	211.7	18.09	11.618	229.64
20	sandstone	41.5	2.92	14.123	53.49
21	sandstone	217.9	39.62	5.319	131.5
22	sandstone	91.2	10.56	8.525	76.64
23	sandstone	65.4	5.79	11.206	68.78
24	sandstone	93.9	3.78	24.761	204.85
25	sandstone	42.6	1.22	35.014	130.24
26	sandstone	150.6	14.8	10.079	144.85
27	sandstone	75.4	5.25	14.288	98.2
28	sandstone	93.3	9.74	9.474	85.29
29	sandstone	10	0.4	25.314	22.29
30	sandstone	220.6	8.28	26.589	515.56
31	sandstone	14.1	0.93	15.1232	19.34

32	sandstone	23.6	2.26	10.334	23.18
33	sandstone	58.9	13.27	4.213	31.11
34	sandstone	36.5	4.13	8.728	31.25
35	sandstone	30.3	3.45	8.673	25.81
36	sandstone	40.1	3.96	10.034	38.43
37	sandstone	28.2	1.63	17.3	43.77
38	sandstone	26.2	2.1	12.401	30.08
39	sandstone	10.8	0.59	18.403	17.76
40	sandstone	10.6	0.38	28.021	26.07
41	sandstone	32.3	3.17	10.101	31.12
42	sandstone	31.3	3.47	8.915	27.25
43	sandstone	18.7	1.46	12.763	22.02
44	sandstone	15.6	0.61	25.643	35.2
45	sandstone	35.6	3.97	8.871	30.87
46	sandstone	33	3.13	10.42	32.63
47	sandstone	38	4.13	9.09	33.6
48	sandstone	17.2	1.33	12.94	20.5
49	sandstone	19.6	1.35	14.483	25.84
50	sandstone	32.5	3.29	9.784	30.5
51	sandstone	25.1	2.12	11.792	27.58
52	sandstone	28.9	1.87	15.382	40.25
53	sandstone	65.2	6.73	9.582	60.16
54	sandstone	132	21.18	6.075	86.74
55	sandstone	45	6.26	7.038	32.75
56	sandstone	54.7	9.3	5.714	34.53
57	sandstone	58.7	10.63	5.345	35.53
58	sandstone	58	9.56	5.905	37.41
59	sandstone	9.8	0.24	40.725	34.76
60	sandstone	63.4	8.65	7.197	46.89
61	sandstone	272.8	11.32	24.061	578.93
62	sandstone	234.8	7.8	30.063	618.34
63	sandstone	222.2	7.54	29.438	573.29
64	sandstone	224.8	7.66	29.301	577.37
65	sandstone	212.5	6.57	32.329	600.78
66	sandstone	252.8	9.7	26.014	578.44

67	sandstone	254.2	10.93	23.229	521.52
68	sandstone	226.4	7.21	31.387	621.84
69	sandstone	267	8.98	29.7	694.85
70	sandstone	163	10.41	15.602	229.99
71	sandstone	49.2	6.09	7.957	39.21
72	sandstone	173.7	14.9	11.57	187.75
73	sandstone	236.1	56.05	3.975	121.03
74	sandstone	193.1	13.83	13.884	245.08
75	sandstone	115.7	9.83	11.681	126.09
76	sandstone	76.9	6.26	12.191	86.98
77	sandstone	72.1	5.48	13.082	86.77
78	sandstone	104.6	16.33	6.251	70.07
79	sandstone	163.5	10.92	14.9	221.19
80	sandstone	110.7	7.26	15.174	152.27
81	sandstone	98.8	8.09	12.125	111.22
82	sandstone	103.6	10.63	9.643	96.08
83	sandstone	104.2	13.39	7.652	80.62
84	sandstone	44.2	3.39	12.972	52.8
85	sandstone	61.0	5.75	10.51	60.76
86	sandstone	48.2	2.87	16.759	72.64
87	sandstone	99.5	7.39	13.379	122.17
88	sandstone	162.1	16.47	9.741	151.59
89	sandstone	102.1	5.82	17.498	160.18
90	sandstone	110.3	6.33	17.382	171.97
91	sandstone	86.7	4.38	19.734	152.28
92	sandstone	279.7	25.21	11.004	289.61
93	sandstone	306.5	23.24	13.115	369.71
94	sandstone	218.7	12.46	17.493	343.01
95	sandstone	337.7	15.45	21.812	652.31
96	sandstone	72.7	3.8	19.065	123.6
97	sandstone	109.2	15	7.145	80.33
98	sandstone	28.9	3.93	7.216	21.41
99	sandstone	111.9	14.21	7.748	87.39
100	sandstone	116.4	5.86	19.813	205.21
101	sandstone	104.9	5.88	17.793	167.16

102	sandstone	119.2	7.18	16.551	177.59
103	sandstone	49.9	6.91	7.087	36.49
104	sandstone	54.8	1.56	35.107	167.97
105	sandstone	93.8	2.75	34.034	278.89
106	sandstone	17.1	0.97	17.579	26.94
107	sandstone	70.8	7.68	9.115	62.74
108	sandstone	64.8	5.02	12.824	76.63
109	sandstone	111.8	8.6	12.925	133.12
110	sandstone	62.9	9.64	6.37	42.68
111	sandstone	125.2	5.44	22.963	254.04
112	sandstone	45.0	3.04	14.754	60.34
113	shale	242.0	39.35	5.988	157.52
114	shale	181.9	40.14	4.311	97.26
115	shale	99.2	30.5	2.945	44.43
116	shale	106.3	31.44	3.085	48.52
117	shale	124	27.16	4.345	66.58
118	shale	162.6	34.66	4.479	88.77
119	shale	220.3	44.09	4.797	125
120	shale	220.6	33.85	6.364	149.59
121	shale	184.7	25.29	7.164	136.14
122	shale	154	17.56	8.655	130.97
123	shale	84.5	5.35	15.737	120.17
124	shale	185.0	26.47	6.848	132.02
125	shale	190.2	27.28	6.83	135.48
126	shale	175.0	21.34	8.078	141.07
127	shale	193.9	26.86	7.082	141.74
128	shale	112.0	23.52	4.555	61.71
129	shale	107.9	26.9	3.762	53.83
130	shale	78.8	15.73	4.808	44.77
131	shale	57.4	11.15	4.959	33.21
132	shale	66.8	13.15	4.886	38.31
133	shale	93.2	22.07	3.986	47.84
134	shale	99.3	21.88	4.318	53.14
135	shale	58.0	8.08	7.043	42.23
136	shale	80.4	13.76	5.672	50.52

137	shale	66.9	4.21	15.826	95.64
138	shale	25.9	2.23	11.509	27.87
139	shale	28.7	3.72	7.568	22.02
140	shale	100.3	9.45	10.517	99.96

Table 3

Published Values of Triaxial Parameters for Hoek-Brown Criterion Using Data Set for Metamorphic Rocks with the Calculated Transition Stress (Sheorey, 1997)

NO	Rock name	σ_c (MPa)	σ_t (MPa)	m_i	σ_{TR}
1	shist	133.6	6.59	20.246	240.41
2	slate	148.6	18.64	7.844	117.14
3	slate	108.7	28.66	3.528	52.60
4	slate	53.4	27.5	1.428	19.35
5	slate	62.3	21.7	1.98	24.42
6	slate	98.0	41.56	1.933	38.16
7	slate	129.4	39.96	2.930	57.84
8	slate	178.3	19.97	8.819	153.89
9	slate	57.8	1.86	30.965	156.67
10	slate	14.5	0.64	22.700	29.10
11	slate	44.2	4.6	9.504	40.51
12	slate	68.1	4.03	16.853	103.17
13	slate	155.1	10.85	14.217	201.10
14	slate	167.6	12.22	13.644	209.42
15	gneiss	315.1	17.58	17.865	504.00
16	gneiss	75.3	13.63	5.343	45.57
17	gneiss	221.7	13.61	16.233	324.43
18	gneiss	195.4	29.86	6.389	132.85
19	gneiss	197.7	22.29	8.759	169.72
20	gneiss	106.4	11.17	9.423	96.84
21	quartzite	144.5	19.28	7.363	108.66
22	quartzite	657.6	21.82	30.102	1733.95
23	quartzite	219.0	13.88	15.71	311.05